CALIFORNIA PATH PROGRAM
INSTITUTE OF TRANSPORTATION STUDIES
UNIVERSITY OF CALIFORNIA, BERKELEY

GPS-Aided Gyroscope-Free Inertial Navigation Systems

Sungsu Park
Chin-Woo Tan

California PATH Research Report
UCB-ITS-PRR-2002-22

This work was performed as part of the California PATH Program of the University of California, in cooperation with the State of California Business, Transportation, and Housing Agency, Department of Transportation; and the United States Department of Transportation, Federal Highway Administration.

Report for TO 4224

June 2002

ISSN 1055-1425

GPS-Aided Gyroscope-Free Inertial Navigation Systems

Sungsu Park and Chin-Woo Tan
PATH, University of California at Berkeley
sungsu@path.berkeley.edy, tan@robotics.eecs.berkeley.edu

PATH Task Order 4224

Abstract

A gyroscope-free inertial navigation system uses only accelerometers to compute navigation trajectories. It is a low-cost navigation system, but its output error diverges at a rate that is an order faster than that of a conventional gyroscope-based system. So integration with an external reference system, such as the Global Positioning System, is necessary for long-term navigation applications. In this paper, an integrated GPS and gyroscope-free INS system is designed to achieve stable long-term navigation. The linear and nonlinear error models of a gyroscope-free INS are derived and are used as Kalman filter equations to estimate the errors in the gyroscope-free INS data. The effects of gyroscope-free inertial measurement unit errors are also analyzed. By using computer simulations, the performance of the integrated GPS and gyroscope-free INS system is verified.

Keywords

INS, GPS, gyroscope-free, MEMS accelerometer, INS error dynamics

Nomenclature

$\{i\}$: inertial frame.
$\{e\}$: earth centered earth fixed frame.
$\{b\}$: body frame.
$\{n\}$: navigation frame.
$\{c\}$: computer frame.
u^a: vector $\vec{u}$ coordinatized in frame $\{a\}$.
$\dot{u}^a$: time derivative of vector $\vec{u}$ in frame $\{a\}$, coordinatized in frame $\{a\}$.
$[u\times]$: skew symmetric matrix corresponding vector u.
ω_{ab}^c: angular rate of frame $\{b\}$ with respect to frame $\{a\}$, coordinatized in frame $\{c\}$.
C_b^a: direction cosine matrix from frame $\{a\}$ to frame $\{b\}$.
$q_b^a = [q_0\ q_1\ q_2\ q_3]^T$: attitude quaternion from frame $\{a\}$ to frame $\{b\}$.
$(q_b^a)^*$: quaternion conjugate of q_b^a.
$\otimes$: quaternion multiplication.
$u_q^a = [0\ (u^a)^T]^T$

$$[q_b^a] = \begin{bmatrix} q_0 & -q_1 & -q_2 & -q_3 \\ q_1 & q_0 & -q_3 & q_2 \\ q_2 & q_3 & q_0 & -q_1 \\ q_3 & -q_2 & q_1 & q_0 \end{bmatrix}, \quad Q(q_b^a) = \begin{bmatrix} -q_1 & -q_2 & -q_3 \\ q_0 & -q_3 & q_2 \\ q_3 & q_0 & -q_1 \\ -q_2 & q_1 & q_0 \end{bmatrix}$$

$$[q_b^a]^S = \begin{bmatrix} q_0 & -q_1 & -q_2 & -q_3 \\ q_1 & q_0 & q_3 & -q_2 \\ q_2 & -q_3 & q_0 & q_1 \\ q_3 & q_2 & -q_1 & q_0 \end{bmatrix}, \quad S(q_b^a) = \begin{bmatrix} -q_1 & -q_2 & -q_3 \\ q_0 & q_3 & -q_2 \\ -q_3 & q_0 & q_1 \\ q_2 & -q_1 & q_0 \end{bmatrix}$$

1 Introduction

Recent advances in micro-machining technology have made the design and fabrication of MEMS (Micro-Electro-Mechanical-Systems) inertial sensors more affordable. Because MEMS inertial sensors are several orders of magnitude smaller than the conventional ones and can be fabricated in large quantities by batch process, they have great potential of applications in the area of low-cost, medium-performance inertial navigation systems (INS) such as those for car navigation [1]. Commercial products of low-cost, medium-level MEMS acceleometers are available on the market, but functional low-cost MEMS gyroscopes may not be commercialized soon because gyroscopes have more inherent physical complexities than accelerometers. Therefore, there is great motivation

for developing a gyroscope-free INS for low-cost, medium performance application areas. Moreover, a gyroscope-free inertial measurement unit (GF-IMU) also has its own application areas. For example, a GF-IMU can be used as a structural vibration detector, and an additional measurement sensor for a normal INS since it functions as an angular acceleration sensor.

Historically, development efforts for GF-IMU have been continued for over 20 years [2]. Although it was known in theory that a minimum of six accelerometers are required for a complete description of a rigid body motion, six-accelerometer schemes were not realized until J. Chen[3] proposed a cube type GF-IMU which has one accelerometer at the center of each surface of a cube and its sensing direction is along the respective surface diagonal. They showed their scheme is workable as a short-term inertial navigation system. In fact, except for a "measure zero" set of six-accelerometer schemes, any other configurations of six accelerometers will work. They all have the same computational simplicity as the cube type GF-IMU. This work is reported in [4].

The position and velocity estimates of the cube type IMU are obtained by some simple computations ([3],[4]) that involve integration of the accelerometer data. Since the data have errors, the integration processes lead to errors that grow with time. Therefore, it is necessary to estimate and correct the errors in the INS data by using external reference data, such as those from the Global Positioning System (GPS). K. Mostov[5] developed a calibration method for compensating configuration errors in Chen's scheme, and showed that it may be used as a car navigation system by incorporating GPS signals in the way of simply resetting GF-INS generated navigation parameters to GPS generated data. However, since the error growth rate of un-reset parameters remains same as the GF-INS alone system, the error may diverge quickly. Therefore, an integrated GPS/GF-INS system needs to include the *error dynamics* of the INS data so that the errors can be estimated, compensated and bounded.

In this paper, we develop a loosely-coupled GPS/GF-INS integration system by deriving linear and nonlinear error dynamic equations of GF-INS for Kalman filters. This paper is organized as follows. Section II presents basic theory of GF-IMU and derives the GF-INS equations. In section III, an identification method for accelerometer errors and its configuration errors is proposed. In section IV, linear and nonlinear error dynamics of GF-INS are derived and the effects of various errors are analyzed. Section V presents the idea of reducing unknown variables which must be estimated by Kalman filter, and discusses Kalman filter implementation. Section VI gives simulation results and section VII concludes this paper.

2 Gyroscope-Free INS

2.1 Gyroscope-Free Inertial Measurement Theory

Consider the earth-centered inertial frame $\{i\}$ and body frame $\{b\}$ shown in Fig.1. $\vec{R}$ is a position vector from earth center to the body frame center, $\vec{R}_j$ is a position vector from earth center to a location j which is fixed in the body frame, and $\vec{r}_j$ is a position vector from body frame center to the location j. Then, the acceleration of the location j is given by

$$\begin{aligned} \ddot{R}_j^i &= \ddot{R}^i + C_b^i[\omega_{ib}^b\times]^2 r_j^b + C_b^i[\dot{\omega}_{ib}^b\times] r_j^b \\ \ddot{R}_j^i &= f_j^i + g^i \end{aligned} \tag{2.1}$$

where f_j^i is a specific force applied at location j and g^i is gravitational force, with both forces represented in the inertial frame. Assuming that single-axis accelerometer is rigidly mounted at location j with the sensing direction η_j^b, then the accelometer produces output A_j such that

$$\begin{aligned} A_j(r_j^b, \eta_j^b) &= f_j^b \cdot \eta_j^b \\ &= (C_b^i)^T(\ddot{R}_j^i - g^i)\cdot \eta_j^b \\ &= \begin{bmatrix} (r_j^b \times \eta_j^b)^T & (\eta_j^b)^T \end{bmatrix} \begin{bmatrix} \dot{\omega}_{ib}^b \\ f^b \end{bmatrix} + (\eta_j^b)^T[\omega_{ib}^b\times]^2 r_j^b \end{aligned} \tag{2.2}$$

where f^b is a specific force observed at the center of body frame. Now, suppose that m accelerometers are distributed in the body frame and if we lump the accelerometer outputs in a vector form, we obtain

$$A = \begin{bmatrix} A_1 \\ ... \\ A_m \end{bmatrix} = J \begin{bmatrix} \dot{\omega}_{ib}^b \\ f^b \end{bmatrix} + \begin{bmatrix} (\eta_1)^T[\omega_{ib}^b\times]^2 r_1 \\ ... \\ (\eta_m)^T[\omega_{ib}^b\times]^2 r_m \end{bmatrix} \tag{2.3}$$

where $J = \begin{bmatrix} J_1^T & J_2^T \end{bmatrix}$ is called a configuration matrix and is given by

$$J_1 = \begin{bmatrix} (r_1 \times \eta_1) & ... & (r_m \times \eta_m) \end{bmatrix}, \quad J_2 = \begin{bmatrix} \eta_1 & ... & \eta_m \end{bmatrix}$$

Note that we omit the superscript b in r_j^b and η_j^b for notation simplicity. If the configuration matrix J has a left inverse matrix, then it is possible to completely describe a

rigid body motion as follows.

$$\begin{bmatrix} \dot{\omega}_{ib}^b \\ f^b \end{bmatrix} = J^+ A - J^+ \begin{bmatrix} (\eta_1)^T [\omega_{ib}^b \times]^2 r_1 \\ ... \\ (\eta_m)^T [\omega_{ib}^b \times]^2 r_m \end{bmatrix} \tag{2.4}$$

where J^+ is left inverse matrix of J. In theory, a minimum of six accelerometers is necessary for J^+ to exist [4].

For a configuration of six accelerometers, the left inverse J^+ is the inverse of J. The existence of J^+ is thus "almost surely" guaranteed since the set of singular 6×6 matrices form a "measure zero" set in $R^{6\times 6}$. For those invertible J matrices, it is nonetheless computationally inefficient to use (2.4) to compute the angular and linear motions. A simple, computationally efficient, INS algorithm was developed in [4] for all those invertible 6×6 configuration matrices J. Among the invertible J matrices, there is a special cube configuration for which the angular acceleration is a linear combination of the accelerometer outputs ([3], [4]). This will be considered next.

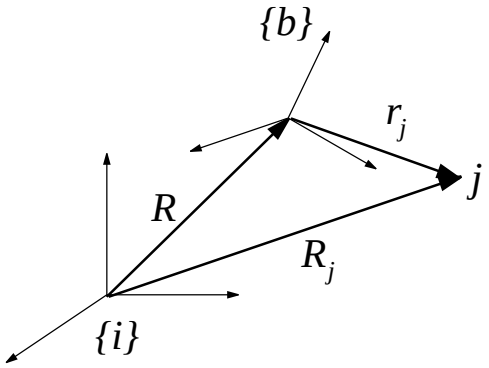

Figure 1: Inertial and body frames

2.2 Cube Type GF-IMU

J. Chen[3] proposed a GF-IMU with six accelerometers. One accelerometer is placed at the center of each of the six cube faces, and its sensing direction is along the respective cube face diagonal in such a way that the six sensing directions form a regular tetrahedron, as shown in Fig.2. With this configuration, equation (2.4) becomes

$$\dot{\omega}_{ib}^b = \frac{1}{2\ell^2} J_1 A \tag{2.5}$$

$$f^b = \frac{1}{2\ell^2} J_2 A + \ell \begin{bmatrix} \omega^b_{ib2}\omega^b_{ib3} \\ \omega^b_{ib1}\omega^b_{ib3} \\ \omega^b_{ib1}\omega^b_{ib1} \end{bmatrix} \tag{2.6}$$

where $2l$ is a cube length. Note that, as it is formulated in [4], equation (2.5)-(2.6) is an input-output dynamical system where A is the input, (2.5) is the state equation and (2.6) is the output equation. Nominal location, sensing direction, and the configuration matrix J_1 and J_2 are given by

$$r_o = \begin{bmatrix} r_{o1} & \cdots & r_{o6} \end{bmatrix} = \ell \begin{bmatrix} 0 & 0 & -1 & 1 & 0 & 0 \\ 0 & -1 & 0 & 0 & 1 & 0 \\ -1 & 0 & 0 & 0 & 0 & 1 \end{bmatrix}$$

$$\eta_o = \begin{bmatrix} \eta_{o1} & \cdots & \eta_{o6} \end{bmatrix} = \frac{1}{\sqrt{2}} \begin{bmatrix} 1 & 1 & 0 & 0 & -1 & -1 \\ 1 & 0 & 1 & -1 & 0 & 1 \\ 0 & 1 & 1 & 1 & 1 & 0 \end{bmatrix}$$

$$J_1 = \frac{\ell}{\sqrt{2}} \begin{bmatrix} 1 & -1 & 0 & 0 & 1 & -1 \\ -1 & 0 & 1 & -1 & 0 & -1 \\ 0 & 1 & -1 & -1 & 1 & 0 \end{bmatrix}$$

$$J_2 = \eta_o$$

From equation (2.5), we see that the angular acceleration of the body frame with respect to the inertial frame is decoupled from the equation of the specific force at the center of body frame, and $\dot{\omega}^b_{ib}$ can be computed from the linear combination of six accelerometer measurements. The angular rate ω^b_{ib} can be obtained by the direct integration of the angular acceleration with a given initial condition. The specific force f^b at the center of body frame is computed from the six accelerometer measurements and the knowledge of an angular rate. Therefore, GF-IMU can perform the same function as a conventional gyroscope-based inertial measurement unit, except for the extra integration of the angular acceleration to obtain the angular rate which is directly measured by the gyroscopes in a conventional gyroscope-based IMU.

2.3 Resolution of Cube-Type GF-IMU

Measurement noises of the accelerometers of GF-IMU limit the minimum detectable signal of angular acceleration and specific force, and thus limit the resolution of angular rate which is calculated by the integration of angular acceleration. Accelerometer noise can be modeled as an uncorrelated zero-mean band-limited white noise, and its power

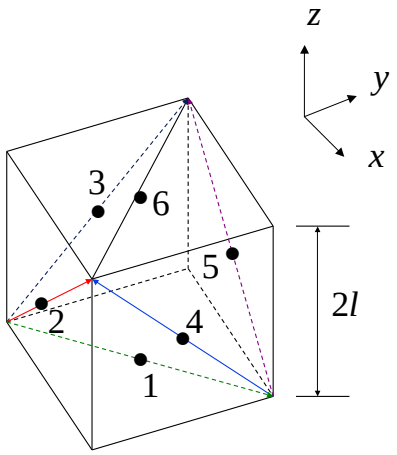

Figure 2: Cube type GF-IMU

spectral density is usually provided by the manufacturer. The standard deviations, or resolution, of the angular acceleration, angular rate and specific force are obtained from covariance calculations. They are given by

$$\begin{aligned}
\sigma_{\omega dot} &= \frac{572.9\sigma_A}{\sqrt{2}\ell} \quad deg/sec^2/\sqrt{Hz} \\
\sigma_{\omega} &= \frac{572.9\sigma_A}{\sqrt{2}\ell}\sqrt{t} \quad deg/sec \\
\sigma_f &\approx \frac{9.8\sigma_A}{\sqrt{2}} \quad m/sec^2/\sqrt{Hz}
\end{aligned} \tag{2.7}$$

where $\sigma_{\omega dot}$, σ_ω and σ_f are the standard deviations of angular acceleration, angular rate, and specific force, respectively. Here σ_A is the standard deviation of the noise of a single accelerometer, and its unit is expressed in $g/\sqrt{Hz}$. Note that the resolution of angular rate grows with time because of integration of the angular acceleration.

2.4 GF-INS Equations

Strapdown inertial navigation system motion equations consist of attitude and velocity differential equations expressed in a navigation frame. Usually, a local level frame is used as a navigation frame. In this work, we use a quaternion as attitude dynamics because of its computational simplicity and easy normalization procedure [6]. The *quaternion differential equation* between the body frame and the navigation frame is given by

$$\dot{q}_b^n = \frac{1}{2}[\omega_{ib}^b]^S q_b^n - \frac{1}{2}[\omega_{in}^n] q_b^n \tag{2.8}$$

where q_b^n is an attitude quaternion that transforms the quaternion vector from its body frame components to its navigation frame components. (The notations in (2.8) are explained in the Nomenclature.)

The *velocity differential equation* in a navigation frame is given by

$$\dot{v}^n = -([\omega_{en}^n \times] + 2[\omega_{ie}^n \times])v^n + C_b^n f^b + g_{ER}^n \tag{2.9}$$

where v^n and g_{ER}^n are the velocity and gravity in a navigation frame, and C_b^n is a rotation matrix from the navigation frame to the body frame. C_b^n can be computed using a quaternion as follows.

$$C_b^n = \begin{bmatrix} 2(q_0^2 + q_1^2) - 1 & 2(q_1 q_2 - q_0 q_3) & 2(q_1 q_3 + q_0 q_2) \\ 2(q_1 q_2 + q_0 q_3) & 2(q_0^2 + q_2^2) - 1 & 2(q_2 q_3 - q_0 q_1) \\ 2(q_1 q_3 - q_0 q_2) & 2(q_2 q_3 + q_0 q_1) & 2(q_0^2 + q_3^2) - 1 \end{bmatrix} \tag{2.10}$$

Equations (2.5), (2.6), (2.8) and (2.9) constitute the gyroscope-free strapdown INS equations. The difference of the GF-INS from the gyroscope-based INS lies in the fact that the output from the GF-IMU is angular acceleration instead of angular rate. With the additional integration step of the angular acceleration, normal gyroscope-based INS algorithms can also be used for the GF-INS. However, incorporation of angular acceleration information into the INS algorithm could achieve faster reaction to a rapid rotational motion.

The position differential equation can be given in different ways depending on the local level frame status. Usually, geodetic positions such as longitude, lateral and height are used for a wide geographical coverage. But for a limited geographical area, the direct integration of v^n along the navigation frame may be used as a position for simplicity with a fixed local level frame. In this case, the *position differential equation* is given by

$$\dot{p}^n = v^n \tag{2.11}$$

Note that in the case when a fixed local level frame is used as a navigation frame, $\omega_{en}^n = 0$ and $\omega_{in}^n = \omega_{ie}^n$, where

$$\omega_{ie}^n \approx \begin{bmatrix} \omega_{ie} \cos\lambda_0 & 0 & -\omega_{ie} \sin\lambda_0 \end{bmatrix}^T$$

and λ_0 is the latitude of the origin of a fixed local frame.

3 Identification of GF-IMU Parameters

The configuration (or misalignment) errors of an accelerometer and the accelerometer errors embedded in the device itself cause detrimental effects on the performance of a GF-INS, so they must be identified and calibrated either off-line or on-line as accurately as possible. We propose an identification procedure of these GF-IMU errors in this section.

The configuration errors of an accelerometer are the location and orientation (or sensing direction) errors of the accelerometer. The error sources of a MEMS accelerometer can be divided into three parts: *scale factor error*, *bias* and *noise*. The resultant erroneous output equation of an accelerometer attached on the j cube surface, $\tilde{A}_j$, can be written by

$$\tilde{A}_j = (1 + s_j)A_j + b_j + w_{aj}, \quad j = 1, ..., 6 \tag{3.1}$$

where s_j is a scale factor error, b_j is a bias, and w_{aj} is a noise. A bias is composed of several components that come from various sources, and is separated into deterministic and stochastic components. A deterministic bias is an offset in a steady state, and a stochastic bias is a remaining random offset after accomplishing deterministic bias compensation. A scale factor error is a sensitivity error. The spectral densities of w_{aj} is given by the manufacturer or can be determined by analyzing the accelerometer output.

For the estimation of the scale factor, bias and sensing direction of the accelerometer on a cube surface, we consider 6 cases of stationary alignment of the GF-IMU cube with respect to a navigation frame: (1) x-axis of a body frame is aligned with the opposite direction of gravity, (2) x-axis of a body frame is aligned with the gravity direction, (3) y-axis of a body frame is aligned with the opposite direction of gravity, (4) y-axis of a body frame is aligned with the gravity direction, (5) z-axis of a body frame is aligned with the opposite direction of gravity, and (6) z-axis of a body frame is aligned with the gravity direction. Then from equations (2.2) and (3.1), the output equations of the

accelerometer in the steady-state are given by

$$\begin{aligned}
\tilde{A}_j^{(1)} &= g_o(1+s_j)\eta_j^T \begin{bmatrix}1\\0\\0\end{bmatrix} + b_j, \quad \tilde{A}_j^{(2)} = g_o(1+s_j)\eta_j^T \begin{bmatrix}-1\\0\\0\end{bmatrix} + b_j \\
\tilde{A}_j^{(3)} &= g_o(1+s_j)\eta_j^T \begin{bmatrix}0\\1\\0\end{bmatrix} + b_j, \quad \tilde{A}_j^{(4)} = g_o(1+s_j)\eta_j^T \begin{bmatrix}0\\-1\\0\end{bmatrix} + b_j \\
\tilde{A}_j^{(5)} &= g_o(1+s_j)\eta_j^T \begin{bmatrix}0\\0\\1\end{bmatrix} + b_j, \quad \tilde{A}_j^{(6)} = g_o(1+s_j)\eta_j^T \begin{bmatrix}0\\0\\-1\end{bmatrix} + b_j
\end{aligned} \tag{3.2}$$

where g_o is the gravity constant. From equation (3.2), a bias is simply estimated by

$$\hat{b}_j = \frac{1}{6}\sum \tilde{A}_j^{(n)} \tag{3.3}$$

We can also use (3.2) to obtain an estimate of the sensing direction. Define the following differences of the measured accelerations:

$$\begin{aligned}
\tilde{A}_j^{(1-2)} = \tilde{A}_j^{(1)} - \tilde{A}_j^{(2)}, \quad \tilde{A}_j^{(3-4)} = \tilde{A}_j^{(3)} - \tilde{A}_j^{(4)}, \\
\tilde{A}_j^{(5-6)} = \tilde{A}_j^{(5)} - \tilde{A}_j^{(6)}, \quad [\tilde{A}_j] = \begin{bmatrix}\tilde{A}_j^{(1-2)} & \tilde{A}_j^{(3-4)} & \tilde{A}_j^{(5-6)}\end{bmatrix}^T
\end{aligned}$$

These differences cancel the bias term and the following relationship is satisfied.

$$\eta_j = \frac{1}{2g_o(1+s_j)}[\tilde{A}_j] \tag{3.4}$$

Since the sensing direction η_j is a unit vector, the denominator in equation (3.4) can be neglected for estimating the sensing direction. Estimation of the sensing direction (in unit vector) for the accelerometer attached to the j cube surface is thus given by:

$$\hat{\eta}_j = \frac{[\tilde{A}_j]}{\sqrt{[\tilde{A}_j]^T[\tilde{A}_j]}} \tag{3.5}$$

The orientation error is η_{ej} and the estimate of this error is $\hat{\eta}_{ej} = \hat{\eta}_j - \eta_{oj}$, where η_{oj} is the nominal (i.e. without error) sensing direction. The orientation error can be determined by two angles, α_1^j and α_2^j, where α_1^j is out-of-plane and α_2^j is in-plane deviation angles of the accelerometer attached to the j cube surface from their nominal sensing direction η_{oj}. The plane referred to here is the j cube surface. (In general, it is the tangent plane

at the location where the accelerometer is attached to.) This plane has a local coordinate system in which the x-axis is aligned with the nominal accelerometer axial direction (i.e. the direction η_{oj} in the body frame) and the z-axis is outward normal direction of the j cube surface. Let C^b_{sj} be a direct cosine matrix that transforms the body frame to the local coordinate frame of the j cube surface. It is then easy to check that η_{ej} is expressed as:

$$\eta_{ej} = C^b_{sj} \begin{bmatrix} \cos\alpha^j_2 \ \cos\alpha^j_1 - 1 \\ \sin\alpha^j_2 \ \cos\alpha^j_1 \\ -\sin\alpha^j_1 \end{bmatrix} \tag{3.6}$$

The estimates of the out-of-plane and in-plane deviation angles are thus given by:

$$\begin{aligned} \hat{\alpha}^j_1 &= -\sin^{-1}(c_{j3}) \\ \hat{\alpha}^j_2 &= \tan^{-1}(\frac{c_{j2}}{c_{j1}+1}) \end{aligned} \tag{3.7}$$

where $c_j = [c_{j1} \ c_{j2} \ c_{j3}]^T = (C^b_{sj})^T \hat{\eta}_{ej}$.

To estimate a scale factor error, we sum each element of $[\tilde{A}_j]$ with the different weighting W_j as follows.

$$W^T_j[\tilde{A}_j] = 2g_o(1+s_j)W^T_j\eta_j \tag{3.8}$$

where the weighting vector W_j is chosen to prevent $W^T_j\eta_j$ from becoming zero. One such choice is:

$$\begin{bmatrix} W_1 & \cdots & W_6 \end{bmatrix} = \begin{bmatrix} 1 & 1 & 1 & 1 & -1 & -1 \\ 1 & 1 & 1 & -1 & 1 & 1 \\ 1 & 1 & 1 & 1 & 1 & 1 \end{bmatrix}$$

The scale factor error is estimated from equation (3.8) as

$$\hat{s}_j = \frac{1}{2g_o W^T_j \hat{\eta}_j} W^T_j[\tilde{A}_j] - 1 \tag{3.9}$$

The location of an accelerometer in the GF-IMU cannot be identified unless the body rotates. So to estimate the location errors, we consider 3 cases of constant speed rotational motion with different alignments of the cube with respect to a navigation frame. In all three cases, the rotation axis is parallel to the gravity direction. The alignment of the cube for each case is such that the rotation axis is in: (1) $x-z$ plane of the body frame, (2) $y-z$ plane of the body frame, and (3) $x-y$ plane of the body frame. The first case is shown in Fig. 3. As shown in the figure, the cube is placed on a wedge of angle β. The combined cube-wedge body is then placed on a rate table for performing the rotations. Assume that the scale factor errors and bias are compensated

through the previous identification procedure. Then from equations (2.2) and (3.1), the accelerometer output equations in a steady-state are as follows:

$$\tilde{A}_j^{(n)} = \eta_j^T f^{b(n)} + \eta_j^T [\omega_{ib}^{b(n)} \times][\omega_{ib}^{b(n)} \times] r_j, \qquad n = 1, ..., 3 \tag{3.10}$$

where

$$\begin{aligned}
\omega_{ib}^{b(1)} &= \omega_0 \begin{bmatrix} \cos\beta & 0 & \sin\beta \end{bmatrix}^T, \quad f^{b(1)} = g_o \begin{bmatrix} \cos\beta & 0 & \sin\beta \end{bmatrix}^T \\
\omega_{ib}^{b(2)} &= \omega_0 \begin{bmatrix} 0 & \cos\beta & \sin\beta \end{bmatrix}^T, \quad f^{b(2)} = g_o \begin{bmatrix} 0 & \cos\beta & \sin\beta \end{bmatrix}^T \\
\omega_{ib}^{b(3)} &= \omega_0 \begin{bmatrix} \cos\beta & \sin\beta & 0 \end{bmatrix}^T, \quad f^{b(3)} = g_o \begin{bmatrix} \cos\beta & \sin\beta & 0 \end{bmatrix}^T
\end{aligned}$$

where ω_0 is an arbitrary nonzero constant angular rate and ω_{ib}^b is the axis of rotation in the body frame. Then the location is estimated by:

$$\hat{r}_j = \begin{bmatrix} \eta_j^T [\omega_{ib}^{b(1)} \times][\omega_{ib}^{b(1)} \times] \\ \eta_j^T [\omega_{ib}^{b(2)} \times][\omega_{ib}^{b(2)} \times] \\ \eta_j^T [\omega_{ib}^{b(3)} \times][\omega_{ib}^{b(3)} \times] \end{bmatrix}^{-1} \begin{bmatrix} \tilde{A}_j^{(1)} - \eta_j^T f^{b(1)} \\ \tilde{A}_j^{(2)} - \eta_j^T f^{b(2)} \\ \tilde{A}_j^{(3)} - \eta_j^T f^{b(3)} \end{bmatrix} \tag{3.11}$$

The existence of the matrix inverse in (3.11) is guaranteed if the rotation axis is not

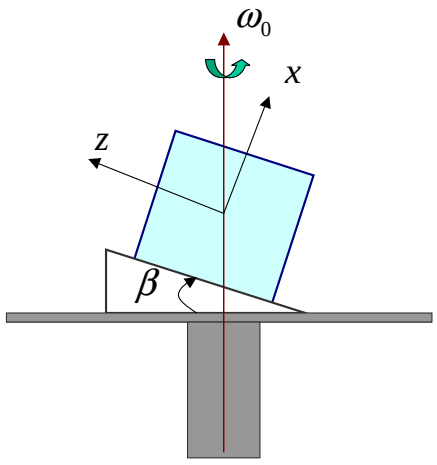

Figure 3: Alignment of Cube

parallel nor orthogonal to the sensing direction of accelerometer j, which corresponds to $\beta = 0°, 45°, 90°$ for the case of nominal accelerometer orientation. The estimation of location error is $\hat{r}_{ej} = \hat{r}_j - r_{oj}$, where r_{oj} is nominal accelerometer location.

4 GF-INS Error Dynamics

4.1 Linearized Error Equations

Strapdown INS error models play an important role in implementing a Kalman filter for an aided navigation system. In this section, we derive a gyro-free strapdown INS error model based on a computer frame approach. If we select the computer frame as a reference frame, the navigation errors are defined as the perturbations in the computer frame. If we perturb equation (2.8), the linearized (first order) additive quaternion errors satisfy the following differential equations.

$$\delta\dot{q}_b^c = \frac{1}{2}([\omega_{ib}^b]^S - [\omega_{ic}^c])\delta q_b^c + \frac{1}{2}Q(q_b^c)\delta\omega_{ib}^b \tag{4.1}$$

Under small tilt angle assumption, the following relationship between quaternion errors and the equivalent tilt angles $\delta\Psi$ can be obtained [6].

$$\delta q_b^c = \frac{1}{2}S(q_b^c)\delta\Psi \tag{4.2}$$

Now, equation (4.1) can be converted to the equivalent tilt angle dynamics as follows.

$$\delta\dot{\Psi} = -[\omega_{ic}^c\times]\delta\Psi + C_b^c\delta\omega_{ib}^b \tag{4.3}$$

For velocity error equations, we perturb equation (2.9) in the computer frame and obtain

$$\delta\dot{v}^c = -([\omega_{ec}^c\times] + 2[\omega_{ie}^c\times])\delta v^c + \delta C_b^c f^b + C_b^c\delta f^b + \delta g_{ER}^c \tag{4.4}$$

In equation (4.4), the attitude error forcing term $\delta C_b^c f^b$ is expressed in terms of a tilt angle as follows:

$$\delta C_b^c f^b = -[f^c\times]\delta\Psi \tag{4.5}$$

For conventional gyroscope-based INS, the angular rate error $\delta\omega_{ib}^b$ in (4.3) and the specific force error δf^b in (4.4) are independent each other. The errors depend on the accuracy characteristics of the gyroscope and accelerometer. In case of a GF-INS, $\delta\omega_{ib}^b$ and δf^b are *correlated* with each other and come indirectly from the same error sources, i.e. accelerometer device errors and the configuration errors in the GF-IMU.

If the scale factor error and bias of each accelerometer are identified with the estimation procedures described in the of previous section, we can apply a compensator to

each accelerometer channel. The compensated accelerometer output $\tilde{A}_j$ is given by

$$\begin{aligned}\tilde{A}_j &= \frac{1}{1+\hat{s}_j}((1+s_j)(A_j+A_{ej})+b_j-\hat{b}_j+w_{aj}) \\ &\approx (1-\delta s_j)(A_j+A_{ej})-\delta b_j+w_{aj}, \quad j=1,...,6\end{aligned} \tag{4.6}$$

where δs_j and δb_j are residual uncompensated errors of the scale factor and bias, and w_{aj} is a random noise. The term A_{ej} is an acceleration error caused by configuration errors and is given by:

$$\begin{aligned}A_{ej} = (\dot{\omega}_{ib}^b)^T(r_j\times\eta_{ej}+r_{ej}\times\eta_{oj})+(f^b)^T\eta_{ej} \\ +(\eta_{oj})^T[\omega_{ib}^b\times]^2 r_{ej}+\eta_{ej}^T[\omega_{ib}^b\times]^2 r_j\end{aligned} \tag{4.7}$$

where r_{ej} is a location error and η_{ej} is a orientation error of the accelerometer attached on the j cube surface. The effect of uncompensated scale factor error can be included as one source of the stochastic bias. Typically, δb_j is modeled as a random walk, i.e. $\delta\dot{b}_j = w_{bj}$. The spectral densities of w_{bj} are determined by analyzing of the compensated accelerometer output at calibration stage. The acceleration error A_{ej} caused by the configuration errors plays a role as a faulty forcing term of the INS algorithms, and needs to be subtracted from accelerometer output before using it as an input data for INS algorithms ([4, 5]). Assume that $\hat{A}_{ej}$ is subtracted from each acceleration channel as follows,

$$\hat{A}_j = A_j + A_{ej} - \hat{A}_{ej} - \delta b_j + w_{aj}$$

where $\hat{A}_{ej}$ is computed with the estimated location and orientation obtained by the identification schemes developed in Section III. The angular acceleration and specific force equations (2.5)-(2.6) will then need to be modified as:

$$\begin{aligned}\dot{\hat{\omega}}_{ib}^b &= \frac{1}{2\ell^2}J_1(A+A_e-\hat{A}_e-\delta b+w_a) \\ \hat{f}^b &= \frac{1}{2}J_2(A+A_e-\hat{A}_e-\delta b+w_a)+\ell\begin{bmatrix}\hat{\omega}_{ib2}^b\hat{\omega}_{ib3}^b \\ \hat{\omega}_{ib1}^b\hat{\omega}_{ib3}^b \\ \hat{\omega}_{ib1}^b\hat{\omega}_{ib1}^b\end{bmatrix}\end{aligned} \tag{4.8}$$

With equations (4.8) and (2.5)-(2.6), the angular rate error differential and specific error equations can be obtained as follows.

$$\begin{aligned}\delta\dot{\omega}_{ib}^b &= \frac{1}{2l^2}J_1(w_a-\delta b-\delta A) \\ \delta f^b &= \frac{1}{2}J_2(w_a-\delta b-\delta A)+l\Omega\delta\omega_{ib}^b\end{aligned} \tag{4.9}$$

where $\delta A = \hat{A}_e - A_e$ is the acceleration error caused from small configuration residual errors after the calibration, and

$$\Omega = \begin{bmatrix} 0 & \omega^b_{ib3} & \omega^b_{ib2} \\ \omega^b_{ib3} & 0 & \omega^b_{ib1} \\ \omega^b_{ib2} & \omega^b_{ib1} & 0 \end{bmatrix}$$

Note that $\hat{A}_e$ is an estimate of the actual error A_e. We can use (3.6) and (4.7) to relate δA to the location and orientation residual errors δr, $\delta\alpha_1$ and $\delta\alpha_2$. We get:

$$\delta A = D\delta c \tag{4.10}$$

where

$$\delta c = \begin{bmatrix} \delta r \\ \delta\alpha_1 \\ \delta\alpha_2 \end{bmatrix}, \quad \delta r = \begin{bmatrix} \hat{r}_{e1} - r_{e1} \\ ... \\ \hat{r}_{e6} - r_{e6} \end{bmatrix}$$

$$\delta\alpha_1 = \begin{bmatrix} \delta\alpha_1^1 \\ ... \\ \delta\alpha_1^6 \end{bmatrix}, \quad \delta\alpha_2 = \begin{bmatrix} \delta\alpha_2^1 \\ ... \\ \delta\alpha_2^6 \end{bmatrix}$$

$$D = \begin{bmatrix} D_1 & D_2 & D_3 \end{bmatrix}$$

$$D_1 = diag\{d_{11}, ..., d_{16}\}, \quad D_2 = diag\{d_{21}, ..., d_{26}\},$$

$$D_3 = diag\{d_{31}, ..., d_{36}\}$$

$$d_{1j} = \eta_j^T[\omega^b_{ib}\times]^2 - (\dot{\omega}^b_{ib})^T[\eta_j\times]$$

$$d_{2j} = ((f^b)^T + r_j^T[\omega^b_{ib}\times]^2 + (\dot{\omega}^b_{ib})^T[r_j\times])C^b_{sj}K_2^j$$

$$d_{3j} = ((f^b)^T + r_j^T[\omega^b_{ib}\times]^2 + (\dot{\omega}^b_{ib})^T[r_j\times])C^b_{sj}K_3^j$$

$$K_2^j = \begin{bmatrix} -\cos\alpha_2^j \ \sin\alpha_1^j \\ \sin\alpha_2^j \ \sin\alpha_1^j \\ -\cos\alpha_1^j \end{bmatrix}, \quad K_3^j = \begin{bmatrix} -\sin\alpha_2^j \ \cos\alpha_1^j \\ \cos\alpha_2^j \ \cos\alpha_1^j \\ 0 \end{bmatrix}$$

If we substitute (4.10) into (4.9), the angular rate error differential and specific force error equations become

$$\begin{aligned} \delta\dot{\omega}^b_{ib} &= \frac{1}{2\ell^2}J_1(w_a - \delta b - D\delta c) \\ \delta f^b &= \frac{1}{2}J_2(w_a - \delta b - D\delta c) + \ell\Omega\delta\omega^b_{ib} \end{aligned} \tag{4.11}$$

Combining equations (4.3), (4.4), (4.5) and (4.11), we have following GF-INS error dynamics.

$$\begin{aligned}
\delta\dot{v}^c &= -([\omega_{ec}^c\times] + 2[\omega_{ie}^c\times])\delta v^c - [f^c\times]\delta\Psi \\
&\quad + \frac{1}{2}C_b^c J_2(w_a - \delta b - D\delta c) + \ell C_b^c \Omega \delta\omega_{ib}^b + \delta g_{ER}^c \\
\delta\dot{\Psi} &= -[\omega_{ic}^c\times]\delta\Psi + C_b^c\delta\omega_{ib}^b \\
\delta\dot{\omega}_{ib}^b &= \frac{1}{2\ell^2}J_1(w_a - \delta b - D\delta c)
\end{aligned} \tag{4.12}$$

4.2 Error Analysis

From the angular rate error differential equation in (4.12), it is desirable to use a larger cube to achieve higher angular acceleration accuracy. But larger cubes may introduce structural flexibility as an error source, and may induce significant high maintenance and operation costs. One apparent problem of small cube is that it is more sensitive to the noise in the accelerometers. For example, if the noise level of acceleometer is on the order of 500 μg resolution, its effect may be negligible for larger cubes. However, for small cube length, for example $\ell = 0.1\ m$, that error can translate to an angular acceleration error of 2.03 deg/sec^2. Thus, as a smaller cube IMU is used, it becomes more important to use high resolution accelerometers.

The effects of configuration errors can be understood by deriving the linearized sensitivity of the accelerometer output with respect to the configuration errors as follows.

$$\begin{aligned}
\frac{\partial A_j}{\partial r_j} &= \eta_{oj}^T[\omega_{ib}^b\times]^2 - (\dot{\omega}_{ib}^b)^T[\eta_{oj}\times] \\
\frac{\partial A_j}{\partial \alpha_1^j} &= -\frac{1}{\ell}((f^b)^T + r_{oj}^T[\omega_{ib}^b\times]^2)r_{oj} \\
\frac{\partial A_j}{\partial \alpha_2^j} &= \frac{1}{\ell}((f^b)^T + r_{oj}^T[\omega_{ib}^b\times]^2 + (\dot{\omega}_{ib}^b)^T[r_{oj}\times])[r_{oj}\times]\eta_{oj}
\end{aligned} \tag{4.13}$$

From equation (4.13), we see that the effects of configuration errors depend on the dynamic motion of the GF-IMU. Generally speaking, as the maneuverability of the motion is higher, the effect of configuration errors gets larger. However, according to the particular dynamics, the configuration errors in each cube surface contribute to the error of accelerometer output at different levels. For example, when translational motion takes place, the location errors in all cube surfaces are totally insensitive. In case of local level plane motion, the orientation errors of the accelerometers on the cube surfaces which are normal to local level plane are hardly detectable. Although some configuration errors have effects on individual accelerometer error, these errors may be inseparable because

each accelerometer error has an effect on INS variables by through the configuration matrix J_1 and J_2. From the point of view of estimation, these inseparable and insensitive errors cause *unobservable* modes and cannot be estimated correctly. However, for some specific vehicle maneuvers with sufficient knowledge of the motion, configuration errors could be estimated as time progresses.

Equation (4.13) suggests the extent of efforts that might be required in estimating configuration errors for specific motions. For example, in car navigation, where the motion is mostly planar and translational, the effect of location errors is very small and we may put less efforts on estimating them. On the other hand, significant efforts should be made on estimating the orientation error for those accelerometers which lie on the cube surfaces that are perpendicular to the motion plane. Equation (4.13) also shows that the effect of a location error is insensitive to cube size in terms of proportional error, whereas that of orientation errors is sensitive to cube size mostly because of specific forces experienced by the GF-IMU.

The error growth rate of GF-INS variables is very rapid compared to that of the gyroscope-based INS. From equation (4.12), the error growth rates of angular rate and specific force, attitude angles, velocity and position are respectively $\sim t$, $\sim t^2$, $\sim t^3$ and $\sim t^4$. Because GF-INS is a rapid diverging system whose divergence rate is an order greater than that of gyroscope-based INS, it is only applicable to short-term navigation unless a reference location system is available to bound the growth of its errors. The Global Positioning System (GPS) is one such system. We will discuss in Section V how a GF-INS can be integrated with the GPS to provide accurate and stable navigation estimates.

4.3 Nonlinear Error Equations

The linearized error dynamics discussed in section IV.A are only valid when errors are small. The small error assumption is well satisfied in very short-term navigation or with fast enough error correction by timely reception of an external signal such as GPS. Since GF-INS is a rapid diverging system, blockage of GPS signal for a few GPS update periods may result in INS errors so large that the linearized error dynamics is no longer valid. In this section, we derive the nonlinear error dynamics by the similar method to X. Kong's[7]. In deriving nonlinear attitude error dynamics, it is more convenient to use multiplicative quaternion and direction cosine matrix errors. The relationship between

multiplicative and additive attitude errors is

$$\begin{aligned} \hat{q}_b^c &\equiv q_b^p = q_c^p \otimes q_b^c = q_b^c + \delta q_b^c \\ \hat{C}_b^c &\equiv C_b^p = C_c^p C_b^c = C_b^c + \delta C_b^c \\ q_c^p &\leftrightarrow C_c^p \end{aligned} \tag{4.14}$$

where p denotes virtual platform frame. Actual attitude quaternion is computed by the following equation in a navigation computer.

$$\dot{\hat{q}}_b^c = \hat{q}_b^c \otimes \hat{\omega}_{cb_q}^b \tag{4.15}$$

If we substitute equation (4.14) to (4.15), we get following multiplicative quaternion error dynamics.

$$\dot{q}_c^p = q_c^p \otimes \delta\omega_{cb_q}^c \tag{4.16}$$

Since $\dot{q}_c^p = q_c^p \otimes \omega_{pc_q}^c$, equation (4.16) is converted to

$$\omega_{pc}^c = \delta\omega_{cb}^c \tag{4.17}$$

where $\delta\omega_{cb_q}^c$ can be calculated by following coordinate transformation:

$$\delta\omega_{cb_q}^c = q_b^c \otimes \delta\omega_{cb_q}^b \otimes (q_b^c)^* \tag{4.18}$$

From the following relation:

$$\omega_{cb_q}^b = \omega_{ib_q}^b - (q_b^c)^* \otimes \omega_{ic_q}^c \otimes q_b^c$$

we can get $\delta\omega_{cb}^b$ as follows.

$$\delta\omega_{cb_q}^b = \delta\omega_{ib_q}^b - (q_b^c)^* \otimes ((q_c^p)^* \otimes \omega_{ic_q}^c \otimes q_c^p - \omega_{ic_q}^c) \otimes q_b^c \tag{4.19}$$

Substituting equation (4.19) to (4.18) gives

$$\delta\omega_{cb_q}^c = (\omega_{ic_q}^c - (q_c^p)^* \otimes \omega_{ic_q}^c \otimes q_c^p) + q_b^c \otimes \delta\omega_{ib_q}^b \otimes (q_b^c)^* \tag{4.20}$$

Equation (4.20) is equivalent to

$$\delta\omega_{cb}^c = (I_3 - (C_c^p)^T)\omega_{ic}^c + C_b^c \delta\omega_{ib}^b \tag{4.21}$$

Since $\omega_{pc}^c = \delta\dot{\Psi}$, we get the nonlinear tilt error dynamics as follows.

$$\delta\dot{\Psi} = (I_3 - (C_c^p)^T)\omega_{ic}^c + C_b^c\delta\omega_{ib}^b \tag{4.22}$$

where C_c^p is a direction cosine matrix composed of 3-2-1 euler angles of $\delta\Psi$. Note that (4.3) is a special case of (4.22) when the tilt angle is small and the linear model becomes valid. From equations (2.9) and (4.14), we have the following *nonlinear velocity error equations*.

$$\delta\dot{v}^c = -([\omega_{ec}^c\times] + 2[\omega_{ie}^c\times])\delta v^c + (C_c^p - I_3)f^c + C_c^pC_b^c\delta f^b + \delta g_{ER}^c \tag{4.23}$$

The position, angular rate and specific force error differential equations remain the same as in the linear case. Therefore, we have following *nonlinear GF-INS error dynamics*.

$$\begin{aligned}
\delta\dot{v}^c &= -([\omega_{ec}^c\times] + 2[\omega_{ie}^c\times])\delta v^c + (C_c^p - I_3)f^c \\
&\qquad + \frac{1}{2}C_c^pC_b^cJ_2(w_a - \delta b - D\delta c) + \ell C_c^pC_b^c\Omega\delta\omega_{ib}^b + \delta g_{ER}^c \\
\delta\dot{\Psi} &= (I_3 - (C_c^p)^T)\omega_{ic}^c + C_b^c\delta\omega_{ib}^b \\
\delta\dot{\omega}_{ib}^b &= \frac{1}{2\ell^2}J_1(w_a - \delta b - D\delta c)
\end{aligned} \tag{4.24}$$

5 Integration of GPS and GF-INS

The Global Positioning System (GPS) provides position and velocity information with no long-term accumulating errors, therefore it has been widely used for an aided sensor for other location systems. A loosely-coupled GPS/INS integration system can be realized in two ways depending on the form of input data to a Kalman filter, that is, either pseudo range/rate differences or three-dimensional position/velocity differences [8]. Since the second type has the advantage of having a simple structure and easier implementation, we consider the second type integration method in this paper, where the difference of INS-generated and GPS-generated positions/velocities is generated as the input to a Kalman filter to form an integrated GPS/INS.

The Kalman filter equation is based on the error dynamics equations, either the linear model (4.12) or the nonlinear model (4.24). In either case, the number of filter states will be 48, which is very large for practical implementation of the filter. We need a reasonable strategy to reduce the number of unknowns because too many unknowns may result in inefficient computations in the filter, especially if the observation yields no significant improvement in the variance of the estimate. Even worse, the type of input errors, such as configuration errors and sensor biases, are poorly estimated under usual

circumstances [9].

From equation (4.10), the j-th element of $D\delta c$ is given by

$$(D\delta c)_j = d_{1j}\delta r_j + d_{2j}\delta\alpha_1^j + d_{3j}\delta\alpha_2^j \tag{5.1}$$

With the assumption that the range of angular acceleration/rate and specific force in the expected maneuvering regimes are estimated a-priori, the effect of configuration errors can be lumped into one common type of error with bias error δb_j, allowing us to reduce the number of unknowns, that is,

$$\begin{aligned} -\delta b_j - (D\delta c)_j &\equiv \delta\bar{b}_j \\ \dot{\delta\bar{b}}_j &= \nu_j \end{aligned} \tag{5.2}$$

where ν_j is a fictitious noise whose intensity is determined by considering the magnitude of bias noise and the expected translational and rotational dynamics for each maneuvering regime experienced by the GF-IMU. For the special case of almost plane and translational motion which is usual case of a car navigation, equation (5.1) is approximated by

$$(D\delta c)_j \approx \frac{1}{\ell}(f^b)^T([r_{oj}\times]\eta_{oj} - r_{oj})\delta\alpha_j \approx d_j\delta\alpha_j$$

where d_j is a number whose nominal value may be known beforehand. Now, the number of filter states is reduced to 18, and is given by

$$\begin{aligned} x = [&\delta p_N\ \delta p_E\ \delta p_D\ \delta v_N\ \delta v_E\ \delta v_D\ \delta\Psi_N\ \delta\Psi_E\ \delta\Psi_D \\ &\delta\omega_{ib1}^b\ \delta\omega_{ib2}^b\ \delta\omega_{ib3}^b\ \delta\bar{b}_1\ ...\ \delta\bar{b}_6]^T \end{aligned}$$

The gravity error in equation (4.12) and (4.24) is approximately given in a local fixed frame by

$$\delta g_{ER}^c \approx \frac{2g_o}{R_e}\delta p_D$$

where R_e is the equatorial radius of Earth [10]. Measurement equations are constructed by the differences between the INS-generated positions/velocities and GPS-generated

positions/velocities, and are given by

$$
\begin{aligned}
z &= \begin{bmatrix} I_3 & 0 & 0 & 0 & 0 \\ 0 & I_3 & 0 & 0 & 0 \end{bmatrix} \begin{bmatrix} \delta p^c \\ \delta v^c \\ \delta \Psi \\ \delta \omega_{ib}^b \\ \delta \bar{b} \end{bmatrix} + \xi \\
&= Hx + \xi
\end{aligned}
\tag{5.3}
$$

where ξ is a measurement noise whose intensity is determined by the GPS performance.

The discrete-time form of filter equation is

$$
\begin{aligned}
x(t_{k+1}) &= f(x(t_k)) + G(t_k)w(t_k) \\
z(t_k) &= Hx(t_k) + \xi(t_k)
\end{aligned}
\tag{5.4}
$$

where subscript k denotes the time update sequence of Kalman filter, and $w(t_k)$ and $\xi(t_k)$ are uncorrelated white noises with covariances $Q(t_k)$ and $R(t_k)$, respectively. Time updates of the state and covariance matrix are

$$
\begin{aligned}
\hat{x}^-(t_k) &= f(\hat{x}(t_{k-1})) \\
P^-(t_k) &= J_f(t_{k-1})P(t_{k-1})J_f^T(t_{k-1}) + G(t_{k-1})Q(t_{k-1})G^T(t_{k-1})
\end{aligned}
\tag{5.5}
$$

where $J_f(t_{k-1})$ is the Jacobian matrix of $f(t_{k-1})$. Until GPS signals are available, only the time update routine is repeated. The Kalman filter gain, state and covariance measurement are updated whenever GPS signals are available as followings.

$$
\begin{aligned}
K(t_l) &= P^-(t_k)H^T(HP^-(t_k)H^T + R(t_l))^{-1} \\
P(t_l) &= (I - K(t_l)H)P^-(t_k) \\
\hat{x}(t_l) &= \hat{x}^-(t_k) + K(t_l)(z(t_l) - H\hat{x}^-(t_k))
\end{aligned}
\tag{5.6}
$$

where t_l denotes the time instance when GPS signals are available, and $x^-(t_k)$ and $P^-(t_k)$ are the last time updates of the state and covariance before GPS signals are available. The state $\hat{x}(t_l)$ is used to correct the INS variables.

If the GPS signal reception is expected to be quite regular, linear error dynamics can be used as the Kalman filter equation. Otherwise, nonlinear error dynamics is preferable, but with a higher computational cost. Both linear and nonlinear dynamics may be used at the same time as Kalman filter equation. By monitoring innovations of Kalman filter, the Kalman filter equation can switch from nonlinear to linear error equation or vice

versa. Multi-model filtering method such as the well-known IMM (interacting multiple model) filter [11] may also be used to cover a wide range of maneuvering regimes by adaptively adjusting the intensity of the lumped fictitious noise in an on-line fashion.

6 Simulation Results

To evaluate the performance of the GPS/GF-INS system, computer simulations are performed. Differential GPS with the accuracy of 10 cm and 0.05 m/sec, latency of 0.1 sec, and accelerometers with a resolution of 200 μg are assumed. IMU-cube length ℓ is 10 cm. The location and orientation errors are assumed to be arbitrarily distributed within the values of ± 1 mm and ± 0.02 deg respectively. The time updates of the INS algorithm, Kalman filter and GPS are $100Hz$, $10Hz$ and $1Hz$, respectively. A vehicle trajectory is used for the simulations. This is shown in Fig. 4, which is a circular motion going up a hill. The GF-IMU experiences a translational maneuvering with the range of $f^b = [(5.1 \sim 5.2) \quad (-1.5 \sim 0.1) \quad (-10.5 \sim -8.4)]^T \ m/sec^2$, and a rotational maneuvering with the range of $\omega_{ib}^b = [(-20 \sim 0) \quad (0 \sim 6) \quad (0 \sim 30)]^T \ deg/sec$ and $\dot{\omega}_{ib}^b = \pm 0.5 \ deg/sec^2$. We assume that GPS signal blockage hardly happens, so the linear error dynamics (4.12) with the common lumped error model (5.2) are used as the Kalman filter equations. The simulation results are presented in Fig. 5. In this figure, position errors in all three dimensions are plotted with their two-sigma bounds, which are about ± 0.15 m for each of north, east and height. The results show that the position errors agree well within the estimated error bounds. For the comparison purposes, the results of those for GF-INS alone and INS-reset-by-GPS systems are also presented in Fig. 6 and Fig. 7. It is clear that the GF-INS alone system loses its navigation capability quickly since the INS errors diverge rapidly. The INS-reset-by-GPS system also has performs poorly compared to the GPS/GF-INS system.

7 Conclusions

We designed an integrated GPS/GF-INS to bound the growing errors of GF-INS which diverge at a rate an order greater than that of gyroscope-based INS. Identification methods for accelerometer device errors and the configuration errors are developed. The linear and nonlinear error dynamics of GF-INS are derived and used for the Kalman filter equation. For the case when the navigation maneuvers are estimated apriori, such as the case for vehicle navigation, the effects of configuration errors and biases can be lumped into one common type of error with fictitious noise whose intensity is determined

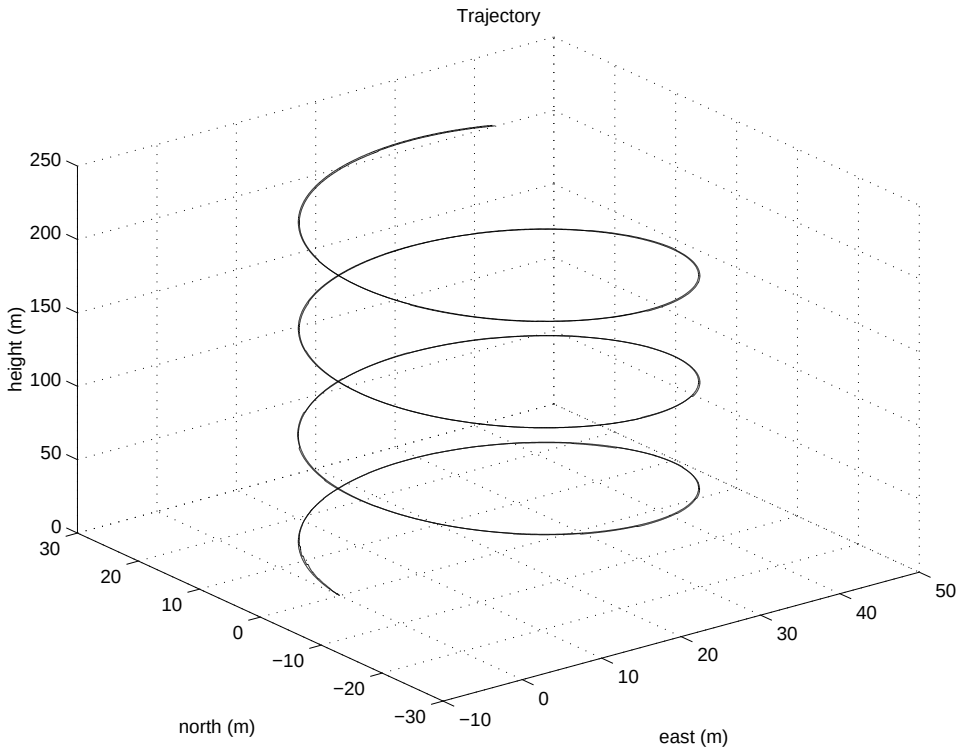

Figure 4: Trajectory

by the magnitude of the expected dynamics experienced by GF-IMU, and thus the order of Kalman filter can be greatly reduced. Since GF-INS is a rapid diverging system, non-linear error model is required when blockage of GPS signals is likely. A decision-based switching scheme or an IMM scheme might need to be implemented to deal with GPS signal blockage or rapidly changing rotational motion. The performance of our integrated system was evaluated using computer simulations. The simulation results show that the performance of the integrated GPS/GF-INS is much superior to that of the previously proposed INS-reset-by GPS system.

Acknowledgements

This work was supported by the New Technology and Research Division of the California Department of Transportation.

References

[1] Yazdi, N., Ayazi, F., and Najafi, K., "Micromachined Inertial Sensors", *Proceedings of IEEE*, Vol.86, No.8, August 1998, pp.1640-1659.

[2] Padgaonkar, A.J., Krieger, K.W., and King, A.I., "Measurement of Angular Acceleration of a Rigid Body Using Linear Accelerometers", *Journal of Applied Mechanics, Transaction of the American Society of Mechanical Engineers*, Vol.42, Sep. 1975, pp.552-556.

[3] Chen, J-H., Lee, S-C., and DeBra, D.B., "Gyroscope Free Strapdown Inertial Measurement Unit by Six Linear Accelerometers", *Journal of Guidance, Control, and Dynamics*, Vol.17, No.2, Mar.-Apr. 1994, pp.286-290.

[4] Tan, C-W., Park, S., Mostov, K., and Varaiya, P., "Design of Gyroscope-Free Navigation Systems", *IEEE* 4^{th} *International Conference on Intelligent Transportation Systems*, Oakland, CA, Aug. 2001. pp.286-291.

[5] Mostov, K., *Design of Accelerometer-Based Gyro-Free Navigation Systems*, Ph.D. Dissertation, U.C. Berkeley, 2000.

[6] D. Chung, J.G. Lee, C.G. Park and H.W. Park, "Strapdown INS Error Model for Multiposition Alignment", *IEEE Trans. on Aerospace and Electronic Systems*, Vol.32, No.4, Oct. 1996, pp.1362-1366.

[7] X. Kong, E. Nebot and H. Whyte, "Development of a non-linear psi-angle model for large misalignment errors and their application in INS alignment calibration", *Proceedings of the IEEE International Conf. on Robotics and Automation*, Detroit, MI, May 1999, pp.1430-1435.

[8] K.P. Schwarz and M. Wei, "Aided Versus Embedded: A Comparison of Two Approaches to GPS/INS Integration", *Proceedings of IEEE Position, Location and Navigation Symposium*, NY, 1994, pp.314-322.

[9] C. Jekeli, *Inertial Navigation Systems with Geodetic Applications*, de Gruyter, 2000.

[10] J. Farrell and M. Barth, *The Global Positioning System and Inertial Navigation*, McGraw Hill, 1999.

[11] Y. Bar-Shalom and X. Li, *Estimation and Tracking: Principles, Techniques, and Software*, Artech House, 1993.

[12] P.G. Savage, "Strapdown Inertial Navigation Integration Algorithm Design Part1: Attitude Algorithms", *Journal of Guidance, Control, and Dynamics*, Vol.21, No.1, Jan.-Feb., 1998, pp.19-28.

[13] P.G. Savage, "Strapdown Inertial Navigation Integration Algorithm Design Part1: Velocity and Position Algorithms", *Journal of Guidance, Control, and Dynamics*, Vol.21, No.2, Mar.-Apr., 1998, pp.208-221.

[14] J. Kim, J. Lee, G. Jee and T. Sung "Compensation of Gyroscope Errors and GPS/DR Integration", *Proceedings of Position, Location and Navigation Symposium*, Atlanta, GA, 1996, pp.464-470.

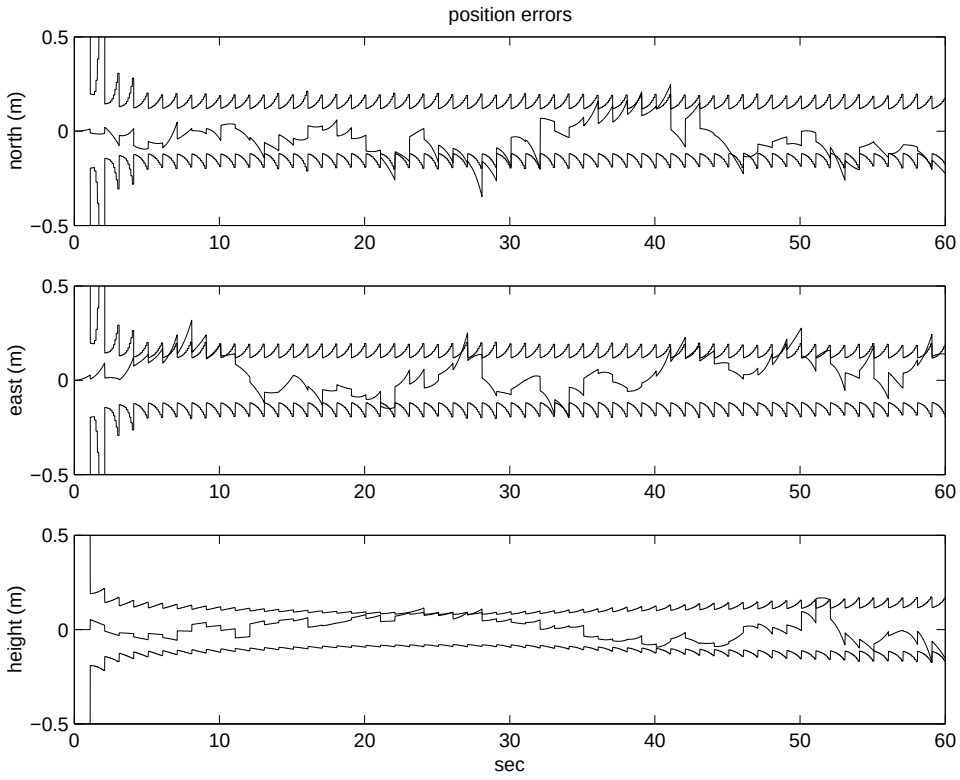

Figure 5: Position errors of GPS/GF-INS

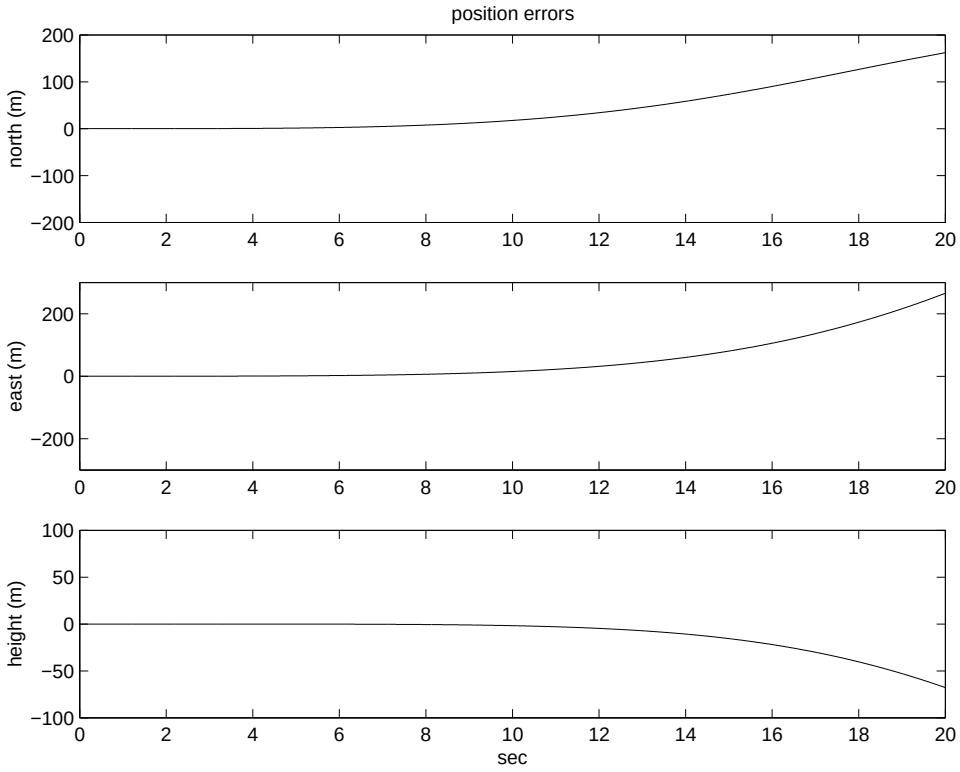

Figure 6: Position errors of GF-INS alone

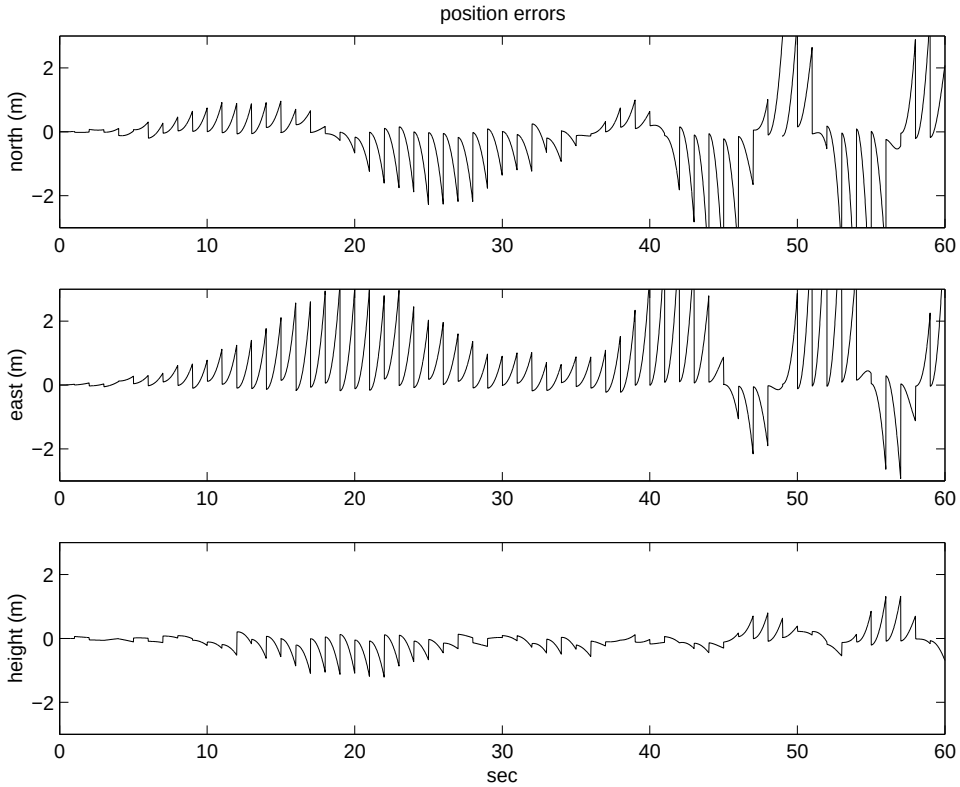

Figure 7: Position errors of GFINS-reset-by-GPS system